

Supporting Information of  
**Surface-sealing encapsulation of phosphotungstic acid in microporous UiO-66 as bifunctional catalyst for transfer hydrogenation of levulinic acid to  $\gamma$ -valerolactone**

Hongzi Tan,<sup>a, b</sup> Siteng Rong,<sup>a</sup> Zhiyuan Zong,<sup>a</sup> Pengrui Zhang,<sup>a</sup> Rongrong Zhao,<sup>a</sup> Feng Song,<sup>a</sup> Hongyou Cui,<sup>a\*</sup> Zhe-Ning Chen<sup>b\*</sup>, Weiming Yi<sup>c</sup> and Fengshan Zhang<sup>d\*</sup>

<sup>a</sup> *School of Chemistry & Chemical Engineering, Shandong University of Technology, Zibo, Shandong 255049, P. R. China.*

<sup>b</sup> *State Key Laboratory of Structural Chemistry, Fujian Institute of Research on the Structure of Matter, Chinese Academy of Sciences, Fuzhou, Fujian 350002, P. R. China.*

<sup>c</sup> *School of Agricultural Engineering and Food Science, Shandong University of Technology, Zibo, Shandong 255049, P. R. China.*

<sup>d</sup> *Shandong Huatai Paper Co. Ltd., Dongying, Shandong 257335, P. R. China.*

## Experiments Section

### 1. Catalyst preparation

**Chemical Materials.** ZrCl<sub>4</sub> (99.5%), terephthalic acid (H<sub>2</sub>BDC, 99%), phosphotungstic acid (PTA, AR), *N,N*-dimethylformamide (DMF, 99.5%), dichloromethane (DCM, 99%), acetic acid (99.5%), pyromellitic dianhydride (PMDA, 99%), tetrakis (4-aminophenyl) methane (TAM, purity, 95%) and petroleum ether (PE, AR) were purchased from Aladdin Chemical Reagent Co. Deionized water was home-made with electrical resistivity of 18 MΩ·cm. All chemical materials in the experiment were used as received without further purification.

**Synthesis of UiO-66.** ZrCl<sub>4</sub> (349 mg, 1.50 mmol) and H<sub>2</sub>BDC (249 mg, 1.50 mmol) were dissolved in 100 mL DMF solution with 92.0 mL acetic acid (1.6 mol) in it. The mixture was then transferred to a 250 mL glass container. The container was capped and placed at 120 °C for 12 h. The white precipitate was washed with DMF three times and soaked in DMF for later use.

**Synthesis of 5%, 10%, 15% and 20% PTA/UiO-66.** Firstly, a certain amount of PTA was dissolved in 20 mL H<sub>2</sub>O and then 200 mg UiO-66 was added. After ultrasonic for 10 min, the mixture was further stirred for 3 h under room temperature. Finally, the solvent was evaporated at 80 °C to obtain PTA/UiO-66 catalyst.

**Synthesis of 15% PTA/UiO-66@PI.** 100 mg of as-synthesized 15% PTA/UiO-66 was redispersed in a mixture of 2.0 mL PMDA DCM solution (0.045mmol, 5 mg/mL) and 122 μL TAM DMF solution (0.0225 mmol, 70 mg/mL) through sonication for 10 min. Then, 35.0 mL PE was poured into the mixture. After stirring for 10 min, 30.0 mL

acetone was added to terminate the polymerization. The obtained purple powder was washed by acetone for three times. Finally, the purple powder was dried and heated at 230 °C for 3 h in N<sub>2</sub> atmosphere to give PTA/UiO-66@PI.

***Synthesis of NaOH pretreated UiO-66.*** 100 mg of pure UiO-66 was dispersed in 200 mL 1 mol·L<sup>-1</sup> of NaOH solution, which was ultrasonic for 10 min and stirred for 5 h under room temperature. The precipitate was washed with H<sub>2</sub>O three times and dried at 60 °C under vacuum condition.

## **2. Catalyst characterization**

Inductively coupled plasma (ICP) spectroscopy was recorded with an Ultima 2 plasma emission spectrometer from Jobin Yvon. Brunauer–Emmett–Teller (BET) surface areas were calculated from the N<sub>2</sub> adsorption-desorption isotherms that were acquired on an ASAP 2020 instrument (Micromeritics) at 77 K. PXRD of all samples were collected by a Rigaku MiniFlex II diffractometer with a Cu K $\alpha$  X-ray source ( $\lambda=1.5406$  Å). Fourier translation infrared (FT-IR) spectroscopy was measured using a Perkin-Elmer Spectrum One FTIR spectrophotometer in the range of 4000-400 cm<sup>-1</sup>. XPS were measured by an ESCALAB 250 Xi spectrometer equipped with an Al anode (K $\alpha$ =1486.6 eV). Transmission electron microscopy (TEM), high angle annular dark field scanning transmission electron microscopy (HAADF-STEM) and high angle annular dark field scanning transmission electron microscopy-energy dispersive X-ray (HAADF-STEM-EDX) mapping were performed on a G<sup>2</sup> F20 field-emission transmission electron microscope (FEI Tecnai) operating at an acceleration voltage of 200 kV. All the catalyst samples were dispersed in ethanol ultrasonically, and then

dropped onto carbon coated copper grids in preparation for the measurements. NH<sub>3</sub> temperature programmed desorption (NH<sub>3</sub>-TPD) was carried out using an Altamira AMI-300 instrument equipped with a thermal conductivity detector. *in situ* pyridine-adsorbed FTIR spectra were used to discriminate acid type of samples on a Thermo fisher Nicolet IS10. Wafers of compressed catalysts samples were mounted in the FTIR cell and degassed in vacuum of 10<sup>-7</sup> Pa at 573 K for 2 h. The samples were saturated with pyridine vapor at 303 K for 10 min to reach an equilibration, and then evacuated at 373 K to remove the excess of probe molecules. The IR spectroscopy were recorded in the range of 400-4000 cm<sup>-1</sup>.

### 3. Catalyst evaluation

Catalytic performance of the prepared catalysts was evaluated in a 100 mL autoclave. Typically, 50 mg of catalyst and 0.2 mol·L<sup>-1</sup> of LA in 50 mL isopropanol were mixed in the reactor under mechanical stirring at 600 rpm. After purged three times with 0.2 MPa of N<sub>2</sub> to expel the air, the autoclave was pressurized with 1.0 MPa of N<sub>2</sub> as reaction atmosphere, and then heated to the desired temperature as the initial point. After reaction, the autoclave was quenched with tap water to room temperature. The products were analyzed by a gas chromatograph (GC, Agilent 6890) equipped with a flame ionization detector and an HP-INNOWAX capillary column (Hewlett–Packard Company, 30 m × 0.32 mm × 0.50 μm). The *n*-hexadecane was used as internal standard. The conversion of LA and the selectivity to product were defined as follows:

$$\text{Conversion}_{LA} (\%) = \frac{(\text{moles of LA})_{in} - (\text{moles of LA})_{out}}{(\text{moles of LA})_{in}} \times 100\%$$

$$Selectivity_{product} (\%) = \frac{(\text{moles of product } i)}{(\text{moles of total product})} \times 100\%$$

Where  $Conversion_{LA}$  and  $Selectivity_{product}$  are the conversion of LA and the selectivity to each product, respectively. There were only two products detected by GC: GVL and isopropyl levulinate (*i*-PL).

#### 4. Calculation details for PTA leaching resistance efficiency

To evaluate the PTA leaching resistance efficiency after polyimide coating, 100 mg of 15% PTA/UiO-66 and 15% PTA/UiO-66@PI catalysts were respectively immersed in 20 mL of deionized water and stirred for 3 h, and the pH values of centrifugal supernatant were measured. The pH value of centrifugal supernatant derived from 15% PTA/UiO-66 dropped by 54.3% (from 7.0 to 3.2), while it only dropped by 2.9% for 15% PTA/UiO-66@PI (from 7.0 to 6.8). In the case of 15% PTA/UiO-66 centrifugal supernatant with pH=3.2, the concentration of  $H^+$  was calculated as  $6.3 \times 10^{-4} \text{ mol} \cdot \text{L}^{-1}$  ( $\text{pH} = -\lg[H^+]$ ), which is equal to  $2.1 \times 10^{-4} \text{ mol} \cdot \text{L}^{-1}$  of dissolved PTA. Similarly, the dissolved PTA in 15% PTA/UiO-66@PI centrifugal supernatant was also calculated as  $5.3 \times 10^{-8} \text{ mol} \cdot \text{L}^{-1}$ , thus the PTA leaching resistance efficiency after polyimide coating was 99.9%.

### Computational methods and models

Here, a cluster model as shown in Figure SX was used to simulate the Zr-oxo species. All geometry optimizations were performed with the density functional theory at the level of dispersion corrected PBE-D3(BJ)<sup>1-3</sup> using the DZP basis sets. Here, the DZP stands for a basis set that employs 6-31G(d) all-electron basis set<sup>4</sup> for H, C and O

atoms, and the corresponding basis sets with the Stuttgart/Dresden effective-core potential (SDD)<sup>5-7</sup> for the Zr atom. Analytical frequencies were calculated to confirm the correctness of the structure of a local minimum. The solvation effects were considered using the SMD model<sup>8</sup> with 2-propanol as the model solvent. Charge analyses are performed by using natural bond orbital (NBO) scheme.<sup>9</sup>

The optimized structures were then adopted to calculate the free energies at the level of M06 functional<sup>10</sup> using TZP basis sets. TZP stands for a basis set that employs a 6-311+G(2d,2p) basis set<sup>11</sup> for the main group elements, and the corresponding basis sets with the Stuttgart/Dresden effective-core potential (SDD)<sup>5-7</sup> for the Zr atom. The free energy at M06/TZP level in solution phase was calculated according to Eq. 1:

$$G_{\text{soln}}^{\text{M06/TZP}} = E_{\text{gas}}^{\text{M06/TZP}} + \Delta G_{\text{thermo(soln)}}^{\text{PBE-D3/DZP}} + \Delta G_{\text{solv}} + RT \ln \left( \frac{RT}{P} \right) \quad (1)$$

The first term in the right-hand side is the electronic energy computed at M06/TZP level in gas phase. The second term is the thermal correction to the free energy of the solute in the solution phase at PBE-D3(BJ)/DZP level. The third term is the solvation free energy. The last term denotes the free energy correction from the gas-phase standard state (1 atm) to the solution phase standard state of 1 M. It should be noted that the solvation free energy  $\Delta G_{\text{solv}}$  was obtained by using SMD model<sup>8</sup> at the level of B3LYP<sup>12-13</sup>/6-31G(d) to make it consistent with the specific methods used in the development of such solvation model. All calculations were carried out using the Gaussian 16 program.<sup>14</sup>

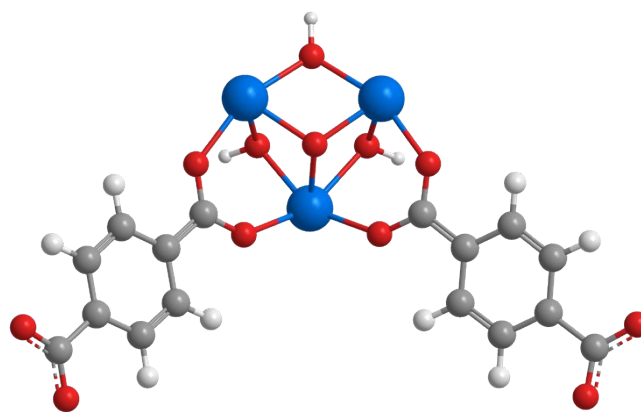


**Figure S1.** Selected cluster model for Zr-oxo cluster.

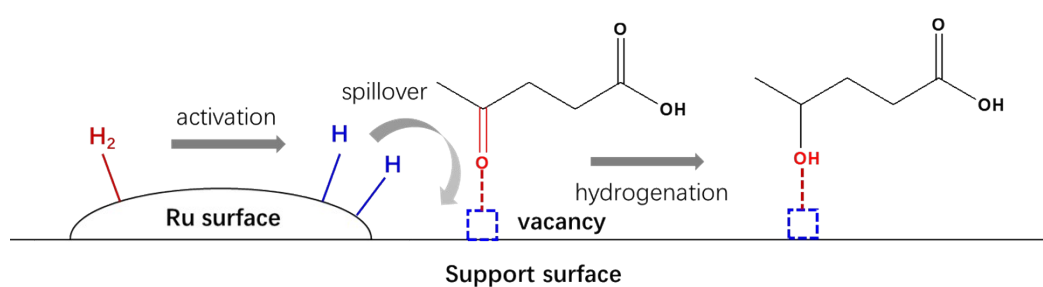


**Figure S2.** Direct hydrogenation of LA with molecular hydrogen catalyzed by Ru species.

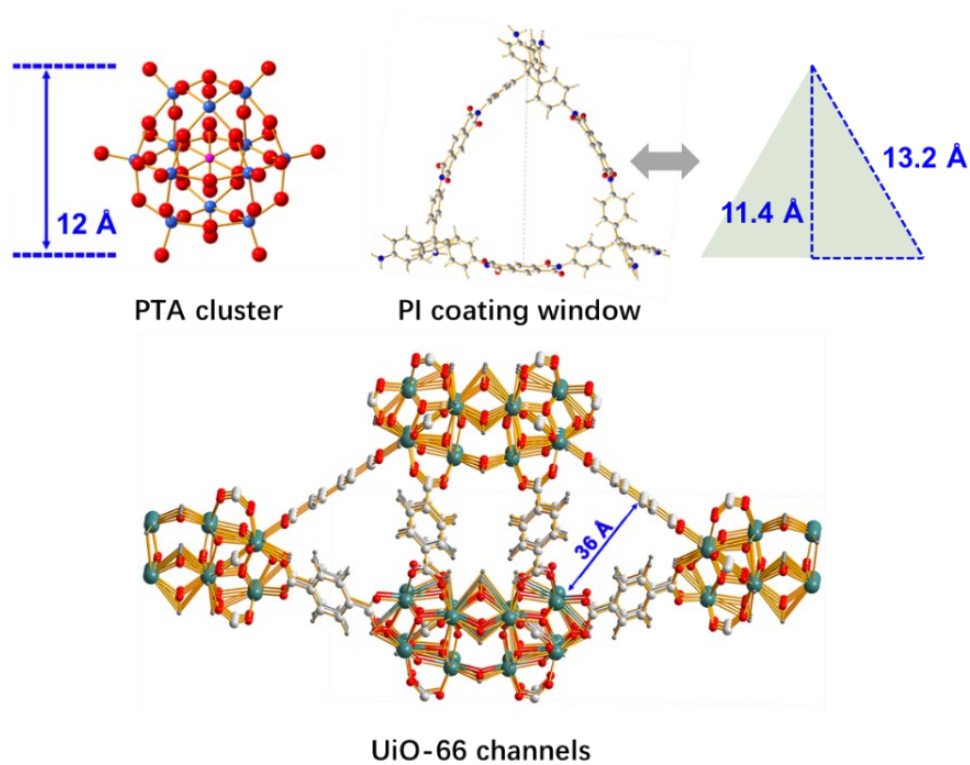


**Figure S3.** Size comparison for PTA cluster, PI coating window and UiO-66 channel.

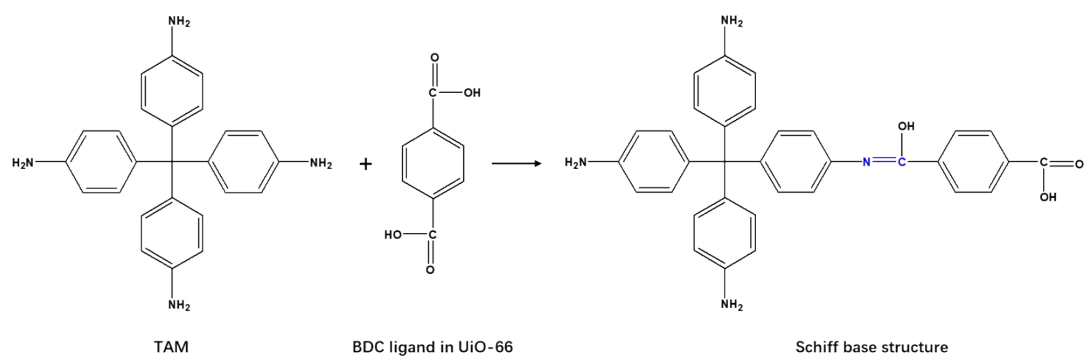


**Figure S4.** Schematic diagram of Schiff base structure generated by TAM and BDC ligands.

**Table S1.** The TON and TOF values of recycled 15% PTA/UiO-66@PI catalyst.

Cycles	1	2	3	4	5
LA moles (mol)	0.01	0.01	0.01	0.01	0.01
LA conversion (%)	100	100	100	100	100
GVL selectivity (%)	93.2	92.1	91.6	93.0	92.5
NaOH volume (mL)	8.1	7.9	8.0	7.9	7.8
PTA moles (mol)	$2.70 \times 10^{-6}$	$2.63 \times 10^{-6}$	$2.67 \times 10^{-6}$	$2.63 \times 10^{-6}$	$2.60 \times 10^{-6}$
TON value	3451.9	3501.9	3430.7	3536.1	3557.7
TOF value ( $s^{-1}$ )	0.32	0.32	0.32	0.33	0.33

**Table S2.** The TON and TOF values of recycled 15% PTA/UiO-66 catalyst.

Cycles	1	2	3	4	5
LA moles (mol)	0.01	0.01	0.01	0.01	0.01
LA conversion (%)	100	100	100	100	100
GVL selectivity (%)	86.4	74.1	43.6	31.7	30.9
NaOH volume (mL)	7.9	7.1	4.5	3.7	3.7
PTA moles (mol)	$2.63 \times 10^{-6}$	$2.37 \times 10^{-6}$	$1.50 \times 10^{-6}$	$1.23 \times 10^{-6}$	$1.23 \times 10^{-6}$
TON value	3285.2	3126.6	2906.7	2577.2	2512.2
TOF value ( $s^{-1}$ )	0.30	0.29	0.27	0.24	0.23

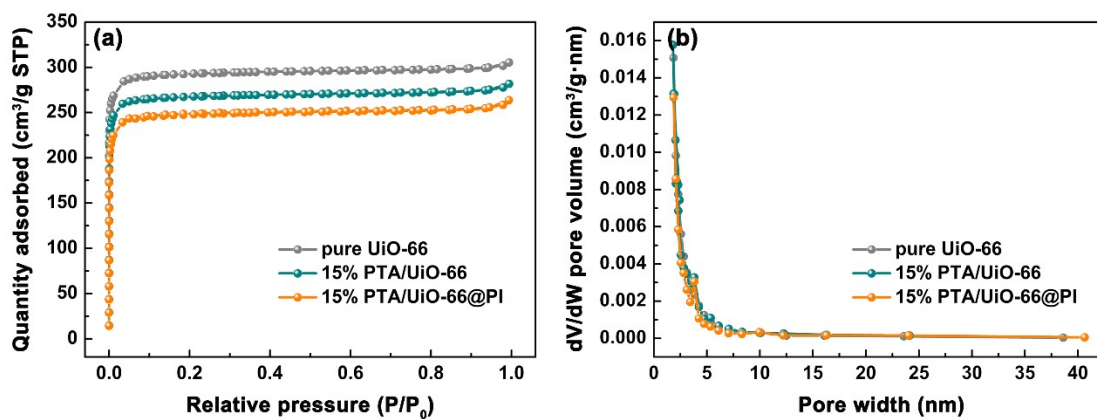


**Figure S5.** (a) N<sub>2</sub> isotherm adsorption-desorption measurements and (b) pore size distribution of pure UiO-66, 15% PTA/UiO-66 and 15% PTA/UiO-66@PI catalysts.

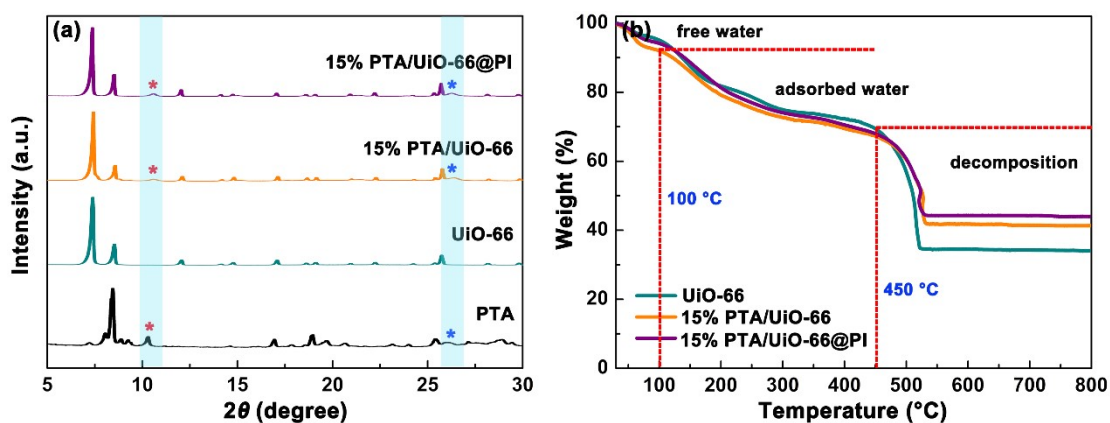


**Figure S6.** (a) PXRD of PTA, UiO-66, 15% PTA/UiO-66, 15% PTA/UiO-66@PI and (b) TGA of UiO-66, 15% PTA/UiO-66, 15% PTA/UiO-66@PI.

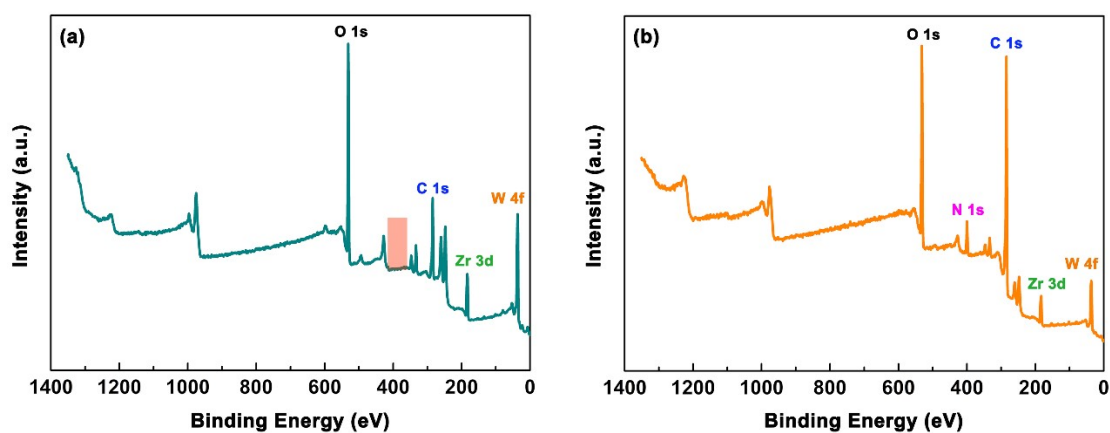


**Figure S7.** XPS spectra of (a) 15% PTA/UiO-66 and (b) 15% PTA/UiO-66@PI.

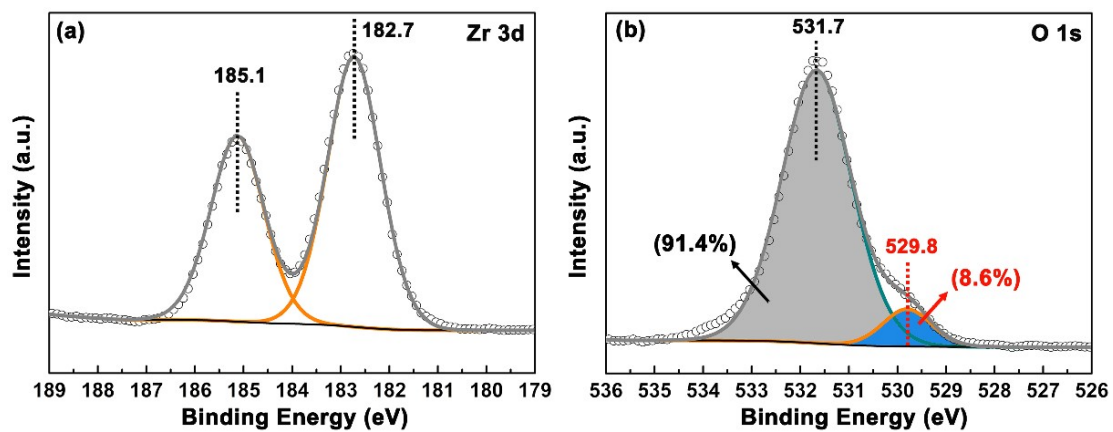


Figure S8. (a) Zr 3d and (b) O 1s XPS spectra of pure UiO-66.

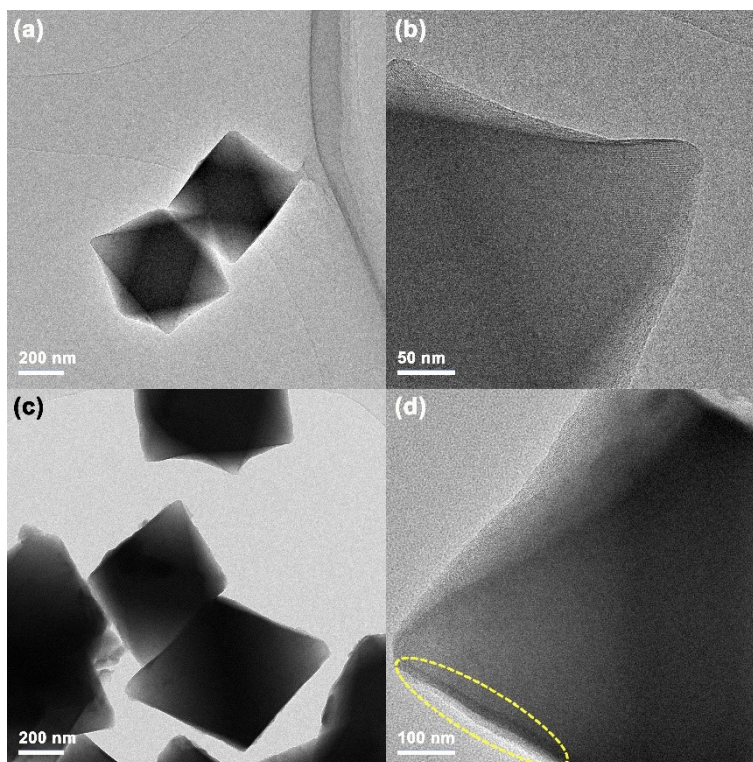


Figure S9. TEM images of (a, b) 15% PTA/UiO-66 and (c, d) 15% PTA/UiO-66@PI.

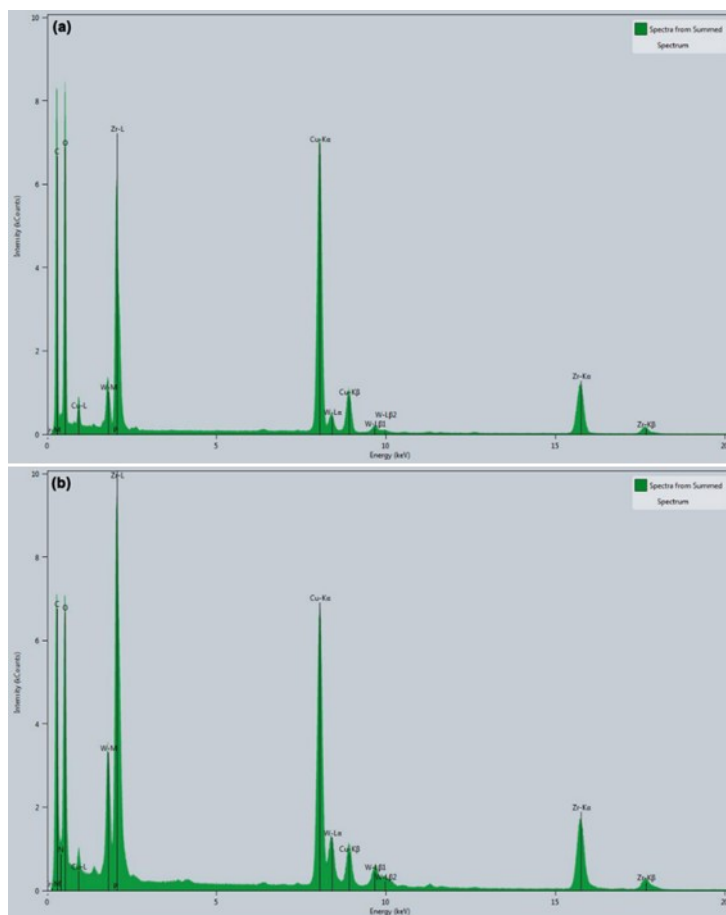


Figure S10. EDS spectra of (a) 15% PTA/UiO-66 and (b) 15% PTA/UiO-66@PI.

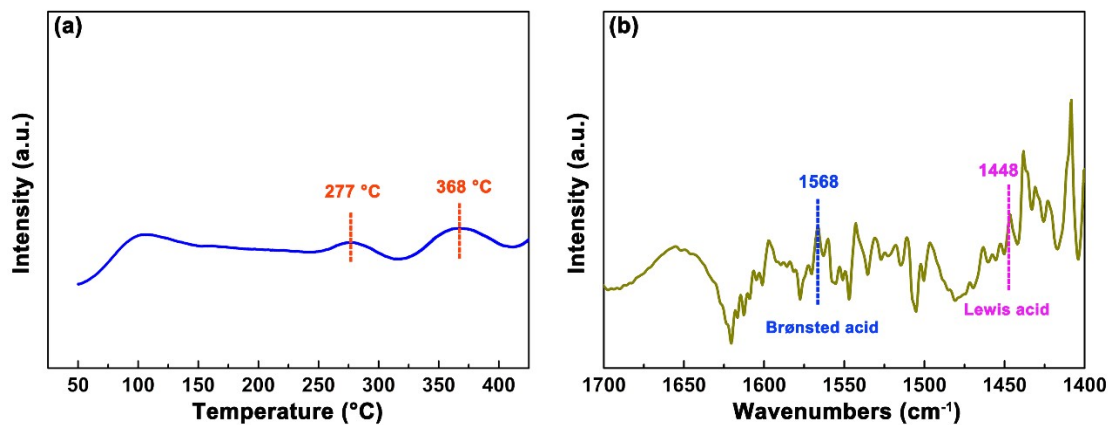
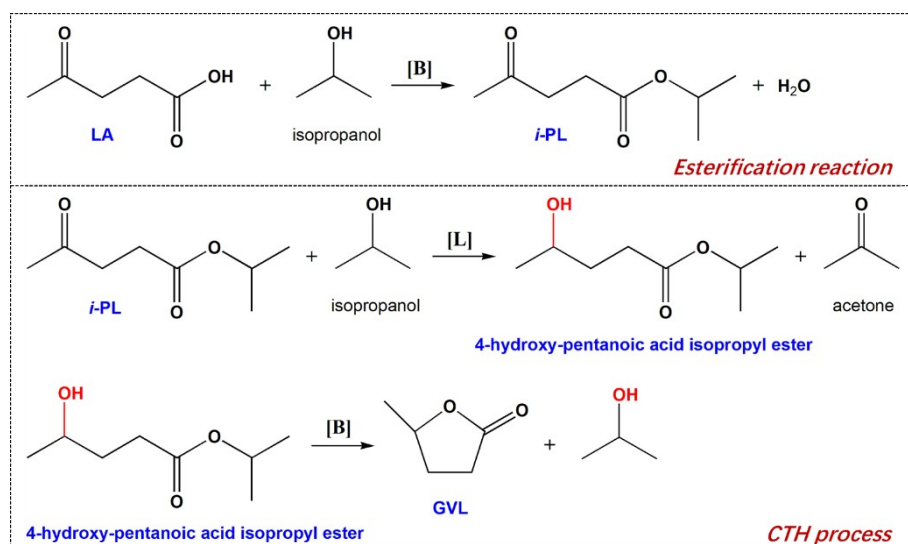
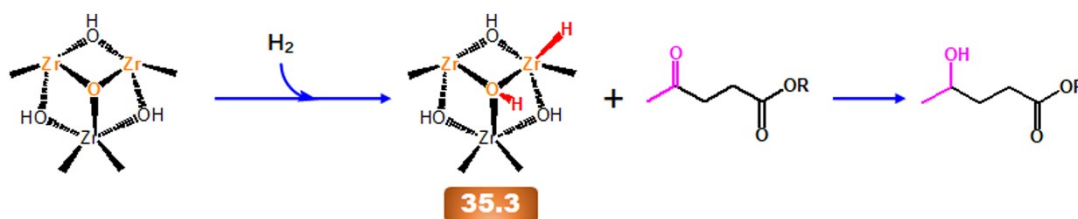


Figure S11. (a)  $\text{NH}_3$ -TPD and (b) Pyridine-IR spectra of PTA/UiO-66@PI.



**Figure S12.** Cascade reactions of LA to GVL via CTH process with isopropanol as hydrogen source.



**Figure S13.** The calculated thermodynamics for carbonyl group hydrogenation in *i*-PL via possible pathway.

## References

- [1] Grimme S.; Antony J.; Ehrlich S.; Krieg H. A consistent and accurate ab initio parametrization of density functional dispersion correction (DFT-D) for the 94 elements H-Pu. *J. Chem. Phys.* **2010**, *132*, 154104.
- [2] Grimme S.; Ehrlich S.; Goerigk L. Effect of the damping function in dispersion corrected density functional theory. *J. Comput. Chem.* **2011**, *32*, 1456-1465.
- [3] Perdew J. P.; Burke K.; Ernzerhof M. Generalized gradient approximation made simple. *Phys. Rev.*

*Lett.* **1996**, *77*, 3865-3868.

[4] Petersson G. A.; Bennett A.; Tensfeldt T. G.; Allaham M. A.; Shirley W. A.; Mantzaris J. A complete basis set model chemistry. 1. The total energies of closed-shell atoms and hydrides of the 1st-row elements. *J. Chem. Phys.* **1988**, *89*, 2193-2218.

[5] Häussermann U.; Dolg M.; Stoll H.; Preuss H.; Schwerdtfeger P.; Pitzer R. M. Accuracy of energy-adjusted quasirelativistic ab initio pseudopotentials. *Mol. Phys.* **1993**, *78*, 1211-1224.

[6] Kuchle W.; Dolg M.; Stoll H.; Preuss H. Energy-adjusted pseudopotentials for the actinides - parameter sets and test calculations for thorium and thorium monoxide. *J. Chem. Phys.* **1994**, *100*, 7535-7542.

[7] Leininger T.; Nicklass A.; Stoll H.; Dolg M.; Schwerdtfeger P. The accuracy of the pseudopotential approximation. 2. A comparison of various core sizes for indium pseudopotentials in calculations for spectroscopic constants of InH, InF, and InCl. *J. Chem. Phys.* **1996**, *105*, 1052-1059.

[8] Marenich A. V.; Cramer C. J.; Truhlar D. G. Universal solvation model based on solute electron density and on a continuum model of the solvent defined by the bulk dielectric constant and atomic surface tensions. *J. Phys. Chem. B* **2009**, *113*, 6378-6396.

[9] Reed A. E.; Weinhold F. Natural bond orbital analysis of near-hartree-fock water dimer. *J. Chem. Phys.* **1983**, *78*, 4066-4073.

[10] Zhao Y.; Truhlar D. G. The M06 suite of density functionals for main group thermochemistry, thermochemical kinetics, noncovalent interactions, excited states, and transition elements: two new functionals and systematic testing of four M06-class functionals and 12 other functionals. *Theor. Chem. Acc.* **2008**, *120*, 215-241.

[11] Krishnan R.; Binkley J. S.; Seeger R.; Pople J. A. Self-consistent molecular-orbital methods .20.

Basis set for correlated wave-functions. *J. Chem. Phys.* **1980**, *72*, 650-654.

[12] Becke A. D. Density-functional exchange-energy approximation with correct asymptotic-behavior.

*Phys. Rev. A* **1988**, *38*, 3098-3100.

[13] Lee C. T.; Yang W. T.; Parr R. G. Development of the colle-salvetti correlation-energy formula into a functional of the electron-density. *Phys. Rev. B* **1988**, *37*, 785-789.

[14] Frisch M. J.; Trucks G. W.; Schlegel H. B.; Scuseria G. E.; Robb M. A.; Cheeseman J. R.; Scalmani G.; Barone V.; Mennucci B.; Petersson G. A.; Nakatsuji H.; Caricato M.; Li X.; Hratchian H. P.; Izmaylov A. F.; Bloino J.; Zheng G.; Sonnenberg J. L.; Hada M.; Ehara M.; Toyota K.; Fukuda R.; Hasegawa J.; Ishida M.; Nakajima T.; Honda Y.; Kitao O.; Nakai H.; Vreven T.; Montgomery J. A.; Peralta J. J. E.; Ogliaro F.; Bearpark M.; Heyd J. J.; Brothers E.; Kudin K. N.; Staroverov V. N.; Kobayashi R.; Normand J.; Raghavachari K.; Rendell A.; Burant J. C.; Iyengar S. S.; Tomasi J.; Cossi M.; Rega N.; Millam J. M.; Klene M.; Knox J. E.; Cross J. B.; Bakken V.; Adamo C.; Jaramillo J.; Gomperts R.; Stratmann R. E.; Yazyev O.; Austin A. J.; Cammi R.; Pomelli C.; Ochterski J. W.; Martin R. L.; Morokuma K.; Zakrzewski V. G.; Voth G. A.; Salvador P.; Dannenberg J. J.; Dapprich S.; Daniels A. D.; Farkas Ö.; Foresman J. B.; Ortiz J. V.; Cioslowski J.; Fox D. J. *Gaussian 16, Revision B. 01*, Gaussian, Inc.: Wallingford, CT, 2016.